Departmental Papers (MEAM)

Department of Mechanical Engineering & Applied Mechanics

12-1-2007

Are diamonds a MEMS' best friend?

Orlando Auciello
Argonne National Laboratory

Sergio Pacheco
Freescale Semiconductor

Anirudha V. Sumant
Argonne National Laboratory

Chris Gudeman
Innovative Micro Technology

Suresh Sampath
Innovative Micro Technology

See next page for additional authors

Author(s)

Orlando Auciello, Sergio Pacheco, Anirudha V. Sumant, Chris Gudeman, Suresh Sampath, Arindom Datta, Robert W. Carpick, Vivekananda P. Adiga, Peter Zurcher, Zhenqiang Ma, Hao-Chih Yuan, John A. Carlisle, Bernd Kabius, Jon Hiller, and Sudarsan Srinivasan

Are Diamonds a MEMS' Best Friend?

Orlando Auciello,
Sergio Pacheco,
Anirudha V. Sumant,
Chris Gudeman,
Suresh Sampath,
Arindom Datta, Robert W. Carpick,
Vivekananda P. Adiga, Peter Zurcher,
Zhenqiang Ma, Hao-Chih Yuan,
John A. Carlisle, Bernd Kabius, Jon Hiller,
and Sudarsan Srinivasan

Next-generation military and civilian communication systems will require technologies capable of handling data, audio, and video simultaneously while supporting multiple RF systems operating in several different frequency bands from the MHz to the GHz range [1]. RF microelectromechanical/nanoelectromechanical (MEMS/NEMS) devices, such as resonators and switches, are attractive to industry as they offer a means by which performance can be greatly improved for wireless applications while at the same time potentially reducing overall size and weight as well as manufacturing costs.

Most MEMS/NEMS devices currently under development are mainly based on silicon because of the available surface machining technology adapted from the silicon-based microelectronics batch fabrication technology [2], [3]. However, silicon has relatively poor mechanical (low Young's modulus of 130 GPa, low hardness of 1,000 kg/mm^2, and fracture strength of 1.3 GPa) [4]–[6] and tribological properties (high adhesion energy or stiction of 106 mJ/m^2) [7] as compared to diamond. Table 1 includes

Orlando Auciello is with the Materials Science Division and Center for Nanoscale Materials at Argonne National Laboratory; Sergio Pacheco and Peter Zurcher are with Freescale Semiconductor; Anirudha V. Sumant is with the Materials Science Division and Center for Nanoscale Materials at Argonne National Laboratory; Chris Gudeman, Suresh Sampath, and Arindom Datta are with Innovative Micro Technology; Robert W. Carpick is with the University of Pennsylvania's Dept. of Mechanical Engineering and Applied Mechanics; Vivekananda P. Adiga is with the University of Pennsylvania's Dept. of Materials Science and Engineering; Zhenqiang Ma and Hao-Chih Yuan are with the University of Wisconsin-Madison's Dept. of Electrical and Computer Engineering; John A. Carlisle is with Advanced Diamond Technologies, Bernd Kabius, and Jon Hiller are with Argonne National Laboratory's Center for Electron Microscopy; and Sudarsan Srinivasan was with the Materials Science Division at Argonne National Laboratory and currently with Intel Corporation.

a number of unique material properties that make diamond an attractive candidate not only for RF MEMS resonator applications but also for MEMS/NEMS devices in general. Chief among these is its combination of bulk properties such as high acoustic velocity, low dissipation, low temperature coefficient of frequency, low charge-trap dielectric, and linear electromechanical response. In addition, surface properties, including low adhesion energy and resistance to tribo-electrical foiling in active electrical contacts, offer the promise of devices that are less sensitive to environmental conditions.

Differently from resonators, RF MEMS switches would not gain in performance due to the high acoustic velocity of diamond. However, diamond does provide certain properties that could potentially enhance the performance of switches. The tribological (low adhesion force) and mechanical properties (high fracture strength) as well as the low-trap characteristics and capability to tailor the conductivity of diamond films could result in possibly higher reliability and lifetimes for such devices. The team is currently in the initial stages of such investigation.

Although the information presented above indicates that diamond is a very good candidate material for some high-performance RF MEMS/NEMS devices, there are several key issues that need to be addressed before diamond can become a reality in commercial MEMS devices, namely: 1) development of the optimum diamond film technology, including growth of diamond layers with high thickness/property uniformity on large area (150 or 200 mm diameter) substrates; 2) development of strategies to integrate diamond with other materials to achieve the multifunctionality required by high-performance RF MEMS/NEMS or MEMS/NEMS in general; 3) development of low-temperature diamond film for integration with CMOS back-end-of-line (BEOL) enabling highly integrated diamond/MEMS/NEMS/CMOS systems [7].

Commercializing Diamond RF MEMS Devices
John A. Carlisle and Neil D. Kane, Advanced Diamond Technologies, Inc.

After decades of research and development, thin-film diamond has finally emerged from the lab and is now accessible to MEMS designers. A number of companies are making various forms of diamond materials available for wafer-scale applications, and diamond is also available as a process module through the MEMS and Nanotechnology Exchange [1]. A great deal of progress has been made to solve the primary technical hurdles of materials integration, surface micromachining, and wafer-scale production. However, the pathway to landing this technology into next-generation wireless systems presents challenges at both the technical and business levels. RF MEMS in general suffers from years of unmet expectations, but OEM RF solutions from Teravicta [2], SiTime [3], Discera [4], and others are just now entering the marketplace. Diamond must work hard to catch up.

The key issues to wide adoption of diamond-based RF MEMS are cost and performance. Regardless of the performance gains diamond enables, to be accepted in the marketplace the price/performance needs to be better than the technologies it's replacing. Diamond's reputation for being expensive is seen as a major obstacle. However, as one step in many, the differential cost incurred by the integration of diamond into the process flow is small and several strategies have been developed to enable diamond to be integrated into complex heterostructures including metals, oxides, and other functional materials. Diamond, which unlike other MEMS materials possesses an extremely stable low stiction surface chemistry, could in fact lower the cost of devices like RF resonators and switches by relaxing some of the need for expensive packaging.

A closely related issue to cost is scalability to wafer-scale production. Until recently state-of-the-art diamond technologies could only uniformly coat wafers 2-3 in. in diameter. Run-to-run variability was also a notorious problem for diamond. Both of these issues have now been resolved thanks to advances in the chemistry and platforms used to synthesize diamond. The UNCD (ultrananocrystalline diamond) technology is particularly interesting in this regard, as it enables films as thin as 100 nm to be routinely deposited on wafers up to 200 mm with excellent thickness and property uniformity. Backend compatibility with CMOS process flow is another major advantage as low temperature (350–400°C) deposition of UNCD films have also been demonstrated. Both diamond-on-silicon (DoSi) and diamond-on-insulator (DOI) UNCD wafers are commercially available now and offer a means by which developers in industry and academia can fabricate prototype devices of their own design for evaluation. These wafers are manufactured using tools and processes that are fully insertable into a MEMS foundry environment and are available in wafers sizes ranging from 100 to 200 mm.

Performance is also a clear driver for diamond. Diamond has a number of intrinsic properties that makes it an ideal candidate for GHz RF MEMS devices including having the highest acoustic velocity of any material, low dissipation (high Q), low temperature coefficient of frequency, and a linear frequency response at high frequencies/powers. Thus, diamond offers a means to enhance performance and achieve a large reduction in form factor via the direct integration of RF filters and switches with high-performance microelectronics. As compelling as a "radio-on-a-chip" is on paper, the smaller area occupied by a RF MEMS front-

This article provides a review describing the work being performed by our team on developing a RF MEMS/NEMS technology based on the ultra-nanocrystalline diamond (UNCD) film technology originallydeveloped and patented at Argonne National Laboratory (ANL). The review will expound on both the science and technology of integrating UNCD into RF MEMS/NEMS systems and also provide preliminary data on working RF MEMS devices using such technology. We address the synthesis and bulk and surface properties of UNCD and its applicability to RF MEMS/ NEMS technology. And we also focus on the specifics of the integration and fabrication processes to create RF MEMS/NEMS devices, including the fabrication and measurement of a low-voltage UNCD-based piezoelectrically driven actuator built at ANL. We also discuss details on the design, fabrication, and performance of a UNCD-based RF MEMS resonator.

Synthesis and Properties of UNCD Films

Synthesis

The fabrication of diamond-based RF MEMS/NEMS devices requires the growth of smooth diamond films with uniform thickness, nanostructure, and properties over large area substrates. There are several flavors of diamond thin films with varying morphology characteristics. Conventional thin-film deposition methods, based on microwave plasma enhanced chemical vapor deposition (MPCVD) with hydrogen-rich chemistry $[H_2(99\%)/CH_4(1\%)]$ produce microcrystalline diamond (MCD) films. This growth process is driven by CH_3^* radicals interaction with the substrate surface, ultimately resulting in carbon atoms inserting into the position corresponding to the diamond lattice. The atomic hydrogen in the plasma preferentially etches a graphitic phase that co-deposits with the diamond phase. However, atomic hydrogen also etches the

end relative to the microprocessor and the differential yield between MEMS and CMOS processes means that it's much more likely that integration of RF components with the digital domain will occur first via 3D integration approaches (SoC, SiP).

Whereas the demonstration of diamond-based devices that have superior performance is relatively straightforward, finding a pathway to landing devices in commercial wireless products is not as clear. Consider that a major goal of the industry (and a major driver for RF MEMS in general) is to integrate some or all of the passive RF components that are currently off-chip. It follows then that both the device technology and the integration strategy must change to meet the needs of the market. Such dramatic changes in system architecture (and the supply chain that feeds them) will not happen overnight, and regardless of the potential performance advantages a new MEMS material like diamond offers, such sweeping changes will happen gradually. The key will be to gain acceptance with internal champions in industry that are responsible for identifying new technologies and inserting them into the development cycle.

For instance, one approach adopted by Advanced Diamond Technologies (ADT) is to introduce diamond RF devices in stages, working with strategic partners that are currently supplying RF devices for frequency reference/timing applications. Specifications for initial market insertion into a targeted OEM socket replacement must be identified for an RF device that will demonstrate the value of diamond on a direct price/performance basis. This is a similar strategy to what SiTime and Discera are following, but whereas they are competing head-to-head with quartz for the

(already commoditized) MHz timing market, ADT is targeting higher-frequency applications. When combined with the availability of DOI from several sources, the global awareness of diamond as a MEMS material will grow in a similar manner to the evolution of SOI as a preferred MEMS platform. The second-stage insertion involves the integration of diamond-based RF filter networks and frequency references with standard ASIC driver modules provided in a form factor suitable for integration via the use of standard packaging. The final stage will require working directly with high-end designers to develop radio-on-a-chip solutions using 3D and direct integration of the diamond-based RF front end with the CPU, time reference, and analog/digital converter.

References

[1] M. Huff, D. Aidala, and J. Butler (Apr. 2006), "MEMS Applications using diamond thin films," Solid State Technol. [online]. Available: http://sst.pennnet.com/Articles/Article_Display.cfm?Section=ARTCL&ARTICLE_ID=253400&VERSION_NUM=2&p=5.

[2] J. McKillop, T. Fowler, D. Goins, and R. Nelson, "Design, performance, and qualification of a commercially available MEMS switch," Teravicta White Paper, [Online]. Available: http://www.teravicta.com/.

[3] P. Gupta, E. Radza, W. Chen, R. Sheridan, R. Sheridan, R. Melamud, M. Lutz, A. Partridge, and K. Petersen, "Leveraging standard IC packaging for MEMS oscillators," SiTime White Paper, [Online]. Available: http://www.sitime.com/news/wph.htm.

[4] W-T. Hsu, "Vibrating RF MEMS for timing and frequency references," in Proc. 2006 Int. Microwave Symp., San Francisco, CA, June 2006, pp. 672–675.

diamond phase, resulting in the formation of inter-granular voids and columnar morphology with large grains ($\geq 1~\mu$m). These grains are much larger than for the UNCD films described in this review [compare Figure 1(a) and Figure 1(b)]. These MCD films exhibit high residual compressive stress, poor intergranular adhesion, and very rough surfaces [8]. Consequently, MCD is ill-suited for producing RF MEMS/NEMS structures with smooth surfaces and sharply defined g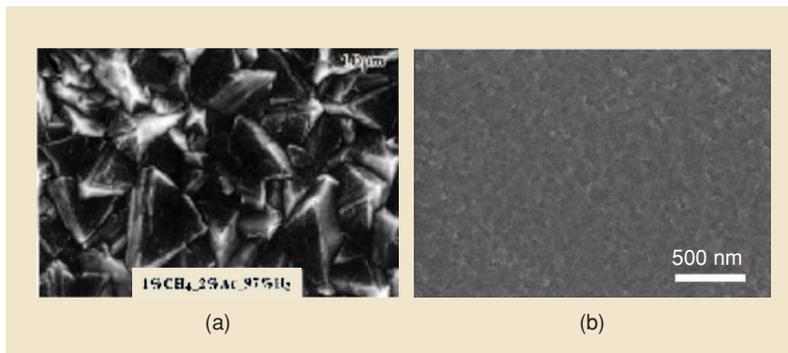eometries. The grain size can be reduced to 50–100 nm, characteristic of films typically known as nanocrystalline diamond (NCD), by increasing the CH_4/H_2 ratio in the plasma. This results in a smoother profile than MCD films, although at the cost of increased nondiamond components at the grain boundaries [8], [9]. There is also another class of NCD with high sp^3 content [10]–[12], which is grown based on the CH_4/H_2 gas chemistry but using a special diamond seeding/nucleation treatment [12]. In this case, the film exhibits the NCD structure as long as the film thickness is limited to less than 100 nm [12]; above that, grain coarsening starts to dominate due to lack of re-nucleation rate and the film grows in a columnar fashion, leading to increase in grain size and roughness with increased film thickness.

In contrast to the growth process for MCD and NCD films described above, the UNCD films discussed in this review are produced by microwave plasma-enhanced chemical vapor deposition (MPCVD) using a novel argon-rich chemistry [Ar (99%)/ CH_4(1%)] with no hydrogen added, [13] which in turn produces carbon dimers (C_2) that play a critical role in the UNCD nucleation process. The dimers together with other hydrocarbon radicals contribute to the growth process. The C_2 dimers insertion into the diamond-seeded surface of the substrate and subsequently into the growing film involves a low energy activation process ($\sim$6 Kcal/mol) for the carbon atoms to establish the bonding characteristic of the UNCD films [14]. A unique outcome of the UNCD nucleation and growth processes is that these films are the only diamond films that can be grown at temperatures as low as 350–400°C [15], paving the way for possible integration into the CMOS BEOL for the development of monolithically integrated UNCD-MEMS/NEMS/CMOS devices.

The UNCD nucleation and growth process results in a unique film microstructure consisting of equiaxed 3–5 nm grains and 0.4-nm wide grain boundaries for plain UNCD [16] [Figure 2(a)] and about 7–10 nm grains and 1–2 nm grain boundaries for UNCD films grown with nitrogen in the gas mixture [Figure 2(b)]. The nitrogen is incorporated in the grain boundaries and acts as a dopant to change the conductivity of the films [17]. The UNCD films exhibit

Property	Silicon	Silicon Carbide	Diamond
Lattice Constant (Å)	5.43	4.35	3.57
Cohesive Energy (eV)	4.64	6.34	7.36
Young's Modulus (GPa)	130	450	1,200
Shear Modulus (GPa)	80	149	577
Hardness (kg/mm²)	1,000	3,500	10,000
Fracture Strength (GPa)	1.0	5.2	5.3
Flexural Strength (MPa)	127.6	670	2,944
Friction Coefficient	0.4–0.6	0.2–0.5	0.01–0.04
Relative Wear Life	1.0		10,000

TABLE 1. Comparison of mechanical and tribological properties between SI, SIC, and diamond.

(a) (b)

Figure 1. *Scanning electron micrographs (SEM) showing (a) the rough morphology of MCD versus (b) the smoother morphology of the UNCD film.*
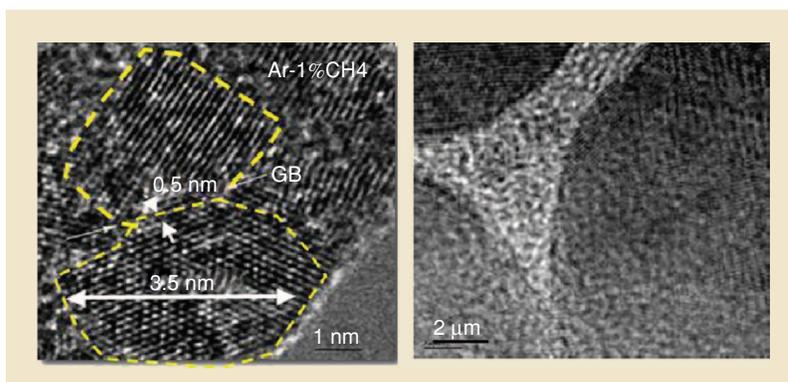

Figure 2. *High resolution transmission electron micrographs (HRTEM) of (a) plain UNCD and (b) nitrogen-grain boundary doped UNCD films produced by MPCVD growth [11].*

pure sp^3 (diamond) carbon bonds in the grains and sp^3/sp^2 mixture in the grain boundaries as revealed by visible and ultra-violet Raman spectroscopy and high-chemical resolution synchrotron-based near-edge X-ray absorption fine structure (NEXAFS) analysis [18], [19]. Thus UNCD is a much smoother film with bulk and surface properties close to those of bulk diamond.

Bulk and Surface Properties

UNCD films exhibit a unique set of complementary mechanical and tribological properties extremely well suited for MEMS/NEMS devices in general. UNCD films exhibit hardness (98 GPa) and Young's modulus (980 GPa) [20] similar to corresponding values for single-crystal diamond (100 GPa and 1,000 GPa, respectively). The Young's modulus is reduced to about 880 GPa [4] when adding about 3% N_2 in the gas phase to the plasma chemistry in order to produce electrically conductive UNCD films. However, this value of Young's modulus is still superior to silicon and other MEMS/NEMS materials (see Table 1).

For RF MEMS resonators, one important figure of merit is acoustic velocity (AV). Diamond has the highest AV of any material, 16,760 m/s, compared to 11,700 m/s for high-quality AlN and 8,100 m/s for single-crystal silicon. This property directly translates to higher frequency of operation for a given geometry but in the same token it allows for larger devices for a given frequency, thus relaxing geometric tolerances and enhancing yield via improved manufacturability. Fixed-free UNCD resonators were fabricated in order to characterize the film's AV and quality factor (Q). The structures were fabricated on 150-mm wafers using 1-μm thick UNCD films grown at 600°C via a proprietary process from Advanced Diamond Technologies (ADT). A vacuum atomic force microscope (AFM) was used for these measurements to avoid damping effects due to air. The length of the cantilevers ranged from 100 μm to 400 μm, but all had a common length-to-width ratio of 7.5. Designed resonant frequencies were in the range of 15 to 300 kHz. The resonant frequency was determined using both a spectrum analyzer and a fast Fourier transform analysis to look at both thermally and piezoelectrically excited vibrations.
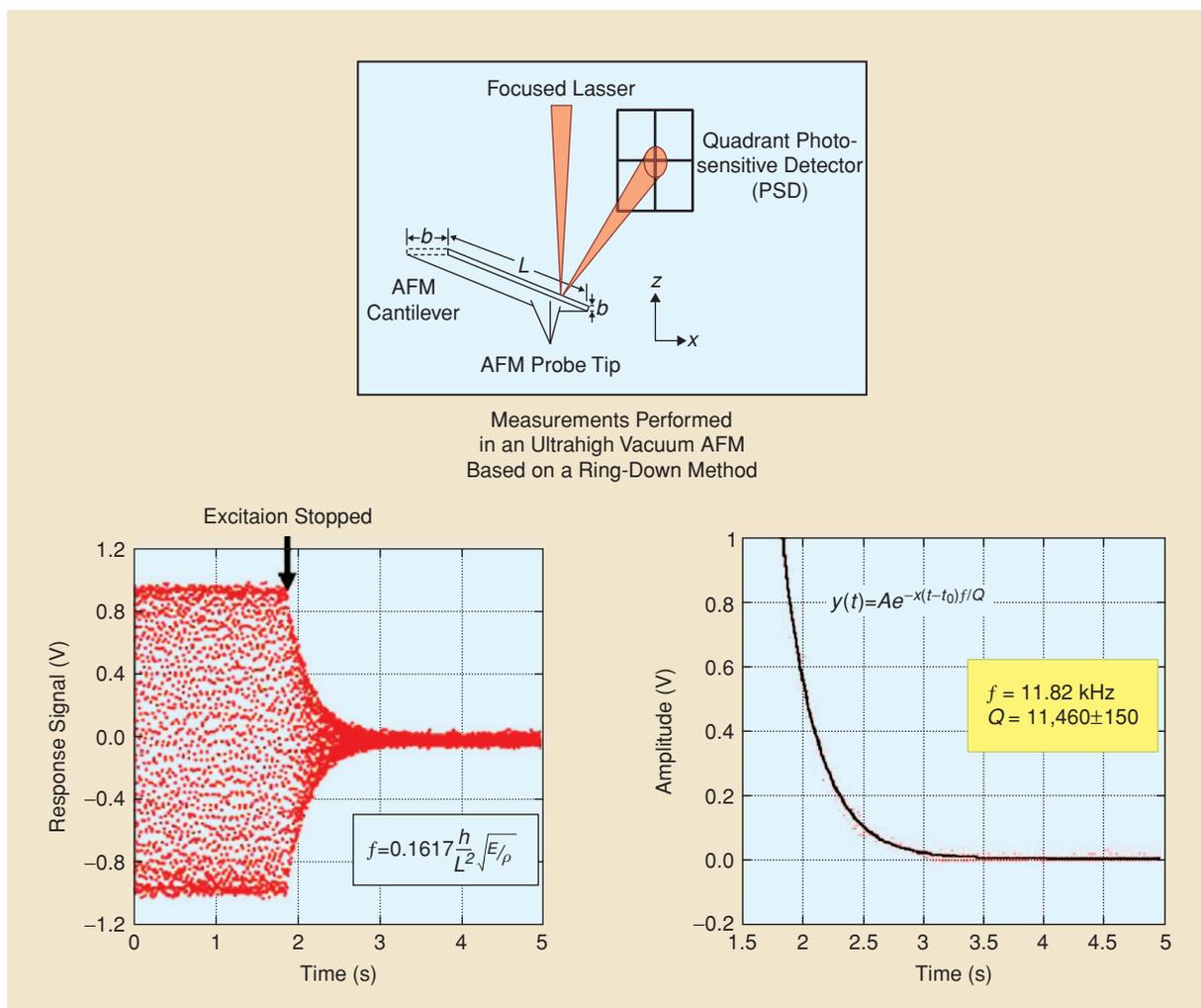
Figure 3. *Measurement setup, excitation, and response for the Q measurement of UNCD cantilevers using an ultrahigh vacuum AFM based on a ring-down method.*

Assuming a 3,500 kg/m^3 mass density for the UNCD films, the Young's modulus E of the films was calculated at 815 GPa, with an acoustic velocity of 15,400 m/s (see Figure 3). A small overhang at the base of the cantilever was not accounted for in these calculations; if included, it would lead to even higher values of E and AV. The quality factor Q of these low-frequency resonators was measured using a ring-down approach and ranged from 10,000 to 13,000. In some cases, significantly lower Q values were found, which can be attributed to the state of the cantilever's surface. Exposing the fixed-free beam surface to atomic hydrogen removes contaminants and nondiamond (amorphous) carbon phases [17], resulting in significant and stable increases in Q, even in air. This is in contrast to silicon resonators, which exhibit increased Q upon oxide removal by vacuum annealing, but only temporarily, due to new oxide formation upon exposure to air or low partial pressures of oxygen [6].

Fracture strength is another important bulk parameter, particularly for MEMS/NEMS devices where moving components are subject to impact. Therefore, the fracture strength of UNCD, and silicon for comparison, was measured using a membrane deflection technique (MDT) developed by Espinosa's Group at Northwestern University [21]. These measurements provide quantitative information on mechanical properties such as Young's modulus, residual stress state, and yield and/or fracture strength. Details on the MDT method can be found elsewhere [4], [5], [21]. The fracture strength of UNCD is about five times larger than for silicon (see Table 1). For RF MEMS contact switches wear can seriously degrade the lifetime of the devices. A thin coating of conductive UNCD could potentially be used to provide longer wear life for such contacting surfaces. Furthermore, the tribological and low-trap characteristics of UNCD could also potentially be used to improve the lifetime of RF MEMS switches by providing an inert surface with a noncharging dielectric. Much work needs to be done in order to verify such hypotheses. The team is in the initial stages of investigating how these UNCD properties impact such RF MEMS switch failure mechanisms.

Regarding surface properties, diamond exhibits surface inertness, a very stable surface chemistry, and low stiction. UNCD has the lowest coefficient of friction (COF) (~0.03–0.05) when compared to silicon (~0.4–0.6), conventional diamond-like carbon (DLC) films (~0.2), and MCD films (~0.4). AFM measurements performed by Carpick's group showed that the top surface of UNCD films deposited over silicon substrates exhibit 11.1 nm rms roughness, while the underside corresponding to the UNCD/silicon interface showed only 2.3 nm rms roughness. AFM studies also provided quantitative information on interfacial adhesion and friction between AFM tips and UNCD film surfaces in ambient air as well as before and after H-plasma treatment [22]. Figure 4(a) shows the work of adhesion between an AFM tip and silicon, UNCD, and single crystal diamond surfaces. Silicon exhibits the highest work of adhesion while the UNCD underside exhibits substantially lower work of adhesion, before H-exposure, than the "passivated" form of silicon (55 mJ/m^2 versus 106 mJ/m^2, respectively). This value for UNCD is comparable to that of the untreated <111> diamond surface. Using the same method, the COF was also measured for both UNCD and diamond <111> surfaces shown in Figure 4(b). The measured friction force for the as-released UNCD underside is comparable to that of the untreated diamond <111> surface. The very low nanoscale adhesion and friction revealed by the plain UNCD surfaces indicate that the underside of UNCD can significantly outperform Si in MEMS/NEMS devices where surface properties are critical for performance.
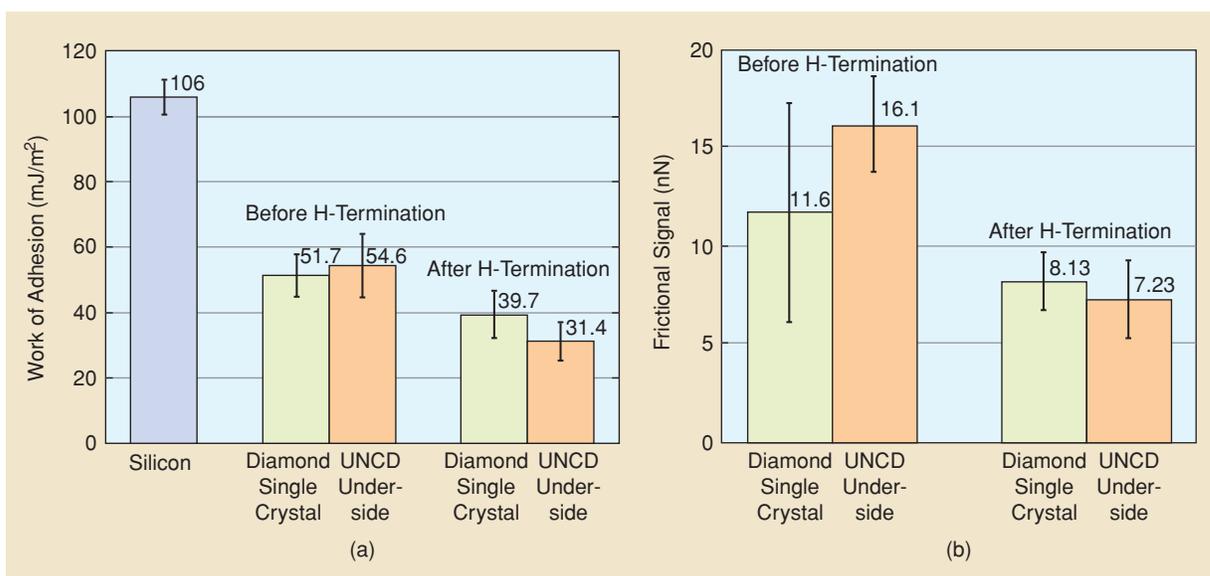
Figure 4. *Graph comparing (a) work of adhesion and (b) friction force of UNCD film underside and single crystal diamond <111> before and after H-termination and solvent-cleaned single-crystal Si [6].*

In conclusion, UNCD exhibits superior mechanical and tribological properties over those of Si and other materials for key MEMS/NEMS devices, particularly for high-frequency systems where AV and stable surface chemistries are key parameters to enable very high-frequency devices in the GHz range.

Electrical Properties

Research at Argonne demonstrated that the electrical conductivity of UNCD films can be tailored from an insulator to practically a semimetal ($\sim 260\Omega^{-1}\cdot cm^{-1}$) depending on the amount of nitrogen incorporated in the UNCD films [23]. This unique electrical conduction phenomenon seems to depend on the combination of the particular grain boundary structure and bonding, including nitrogen incorporation into the grain boundaries [24]. The microstructural changes in nitrogen-doped UNCD films reveal grain size enlargement to ~10 nm from the 2–5 nm characteristic of undoped UNCD, and grain boundary size increase from about 0.4 to 2.2 nm from undoped to doped UNCD [14]. This increase in the grain boundaries also causes a slight reduction in the Young's modulus of the doped UNCD from 980 to 880 GPa. The ability to dial in the electrical conductivity of UNCD provides additional flexibility in the design and realization of RF MEMS devices such as electrostatically driven resonators.

### Materials Integration and Fabrication Process

Two main fabrication processes to produce UNCD-based MEMS/NEMS have been developed, namely, 1) selective seeding and growth, and 2) seeding plus photolithography followed by reactive ion etching (RIE). In both cases, the initial step is a seeding process whereby nanoparticles of diamond are embedded on the surface of the substrate by mechanical polishing or ultrasonic seeding via the exposure of the substrate to a solvent-based suspension of nanodiamond powder in an ultrasonic bath. The fabrication processes then proceed as described below.

MEMS Fabrication Process Using UNCD Layers

Selective Seeding and Growth Process

In this process, the substrate is seeded by 1) using photoresist to prevent exposure of selected areas to the diamond powder, 2) using diamond-loaded photoresist to produce a patterned nucleation layer, or 3) seeding the substrate uniformly and then selectively etching portions of the surface to remove diamond-seeded areas. The feature resolution that can be achieved by this method is limited by the grain size. A schematic of the selective seeding plus UNCD growth process is shown in Figure 5(a). Examples of MEMS structures produced by selective seeding and growth are shown in Figure 5(b) and Figure 5(d) for UNCD-based structures and Figure 5(c) and Figure 5(e) for MCD-based structures. It is clear that the resolution achieved by the UNCD-based process is far superior to that achieved with MCD layers.
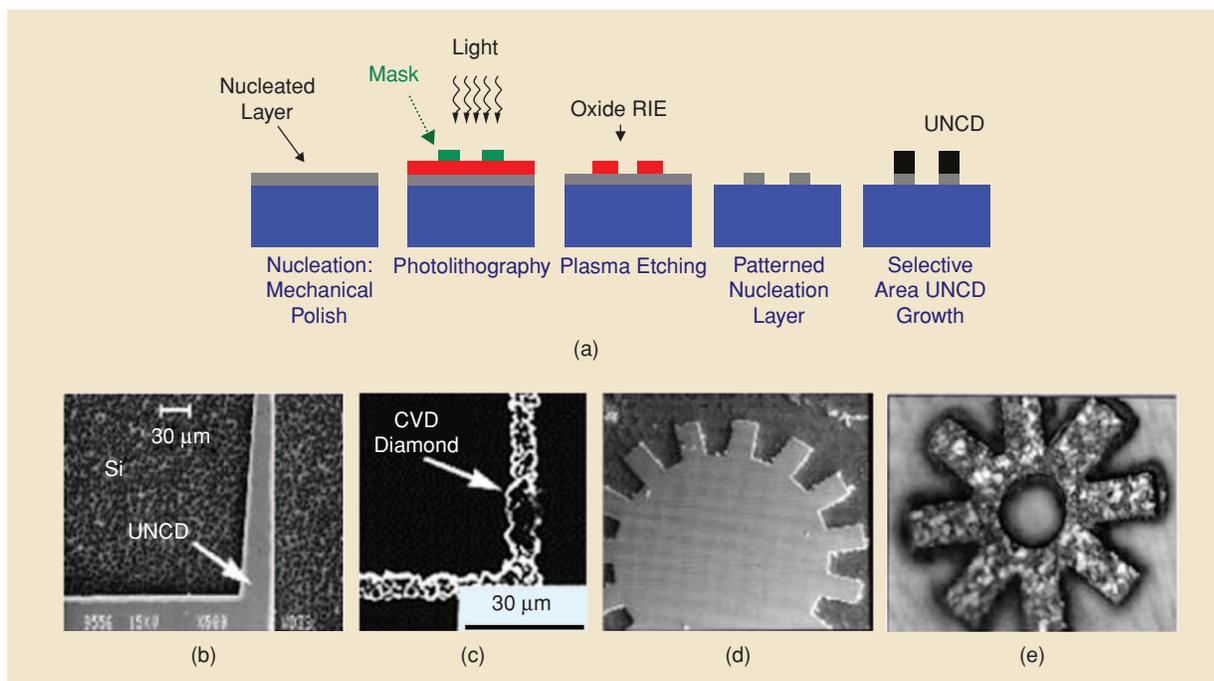
Figure 5. (a) Schematic showing uniform seeding of substrate, followed by photolithography and selectively etching of the substrate surface though vias open in the photoresist layer to remove diamond-seeded areas, and finally UNCD growth on selectively seeded areas; UNCD-MEMS structures grown using the selective seeding plus growth, using the UNCD growth process (b) and (d) and the MCD growth process (c) and (e). It is clear that the UNCD growth process produces MEMS structures with much higher resolution and smoother surface morphology than the MCD process.

Surface Micromachining of UNCD Thin Films

In this fabrication process, blank UNCD layers are typically grown on a sacrificial release layer such as SiO_2, (e.g., thermal, LPCVD). Methods have been reported [25] to force the growth of conventional MPCVD diamond on SiO_2, typically by seeding the SiO_2 surface by ultrasonic abrasion in a diamond powder suspension. Continuous diamond films 15–20 μm thick have been achieved using this method. However, gaps between the film and the substrate are present, and the films are extremely rough [26]. Diamond films grown from CH_4-Ar plasmas are able to form directly on SiO_2 substrates with appropriate diamond seeding processes (see nucleation section below) [14], [15], [23], [27].

It is therefore possible to use SiO_2 as a sacrificial substrate layer for multilayer UNCD devices. As shown in Figure 6(a), a UNCD layer is deposited on a thermal SiO_2 layer, followed by a second SiO_2 layer deposited by CVD. Photoresist is then used to pattern the hard SiO_2 mask using RIE with CF_4/CHF_3 gas mixture (2:1) plasma [Figure 6(b) and Figure 6(c)]. Oxygen plasma is then used to perform RIE etching of the UNCD pattern using the SiO_2 hard mask. Initial measurements of etch rate, although not optimized, indicate that UNCD can

---

Metrology Techniques Glossary for the Characterization of UNCD

AES—Auger Electron Spectroscopy probes the composition and chemistry of a surface by measuring the energy of electrons emitted from that surface when it is irradiated with electrons of energy in the range of 2–50 keV. Some of the electrons emitted from the surface have energies characteristic of the element from which they were emitted and, in some cases, the bonding state of those atoms. The physical process that causes these electrons to be emitted is called the Auger effect. In the Auger effect, an electron is removed from a core level of an atom by an electron bombarding the material. The removed electron leaves a vacancy, which is filled by an electron from a higher level. The decaying electron transfers some of its energy to another electron, which is ejected from the atom; this electron is also known as the Auger electron (http://en.wikipedia.org/wiki/Auger_spectroscopy).

AFM—Atomic Force Microscope is an atomic scale resolution scanning probe microscope, which provides images with resolution 1,000 times better than the optical diffraction limit. The information is gathered by "feeling" the surface by means of a mechanical tip 50–100 nm in diameter, which is integrated on a cantilever (typically silicon or silicon nitride). When the tip contacts the sample surface, forces between the tip and the sample lead to a deflection of the cantilever according to Hooke's law. The cantilever deflection is measured by reflecting a laser beam from the cantilever surface and directing it to an array of photodiodes (http://en.wikipedia.org/wiki/Atomic_force_microscope).

MDT—Mechanical Deflection Technique was developed by Prof. Espinosa at Northwestern University to measure the fracture strength and toughness of materials at the MEMS scale. The technique uses a nanoindenter that applies a line-load to a fix-fix rectangular beam and an interferometer focused on the underside of the membrane to measure deflection. The result is direct tension, in the absence of strain gradients of the gauged regions, with load and deflection being measured independently (http://clifton.mech.northwestern.edu/~espinosa).

NEXAFS—Near-Edge X-ray Absorption Fine Structure Spectroscopy, a synchrotron-based technique, is an element-specific electronic structure probe that directly samples the local density of unoccupied states (LDOS) as well as the orientation of the chemical bonding and the presence of short-range crystalline order. NEXAFS permits extraction of the signal from a surface monolayer or even a single buried layer in the presence of a large background signal. It is not to be confused with EXAFS (Extended X-ray Absorption Fine Structure), which is a structural probe of bond length and orientation, or XANES (X-ray Absorption Near Edge Structure), which is a probe of heavy elements in which multiple scattering effects dominate the absorption process (http://en.wikipedia.org/wiki/NEXAFS).

SEM—Scanning Electron Microscope is capable of producing high-resolution images of the surface topography of a material. In a typical SEM, electrons are thermionically emitted from a cathode and shaped into an electron beam by electromagnetic lenses. The electron beam (typically with 5–100 keV of energy) is focused to a spot size of 1-5 nm on the surface of the sample and scanned in a raster fashion over a rectangular area. The electron beam impacting on the sample surface releases secondary electrons that are detected by a solid-state detector to form an image of the surface (http:// en.wikipedia.org/wiki/Scanning_electron_microscope).

XPS—X-ray Photoelectron Spectroscopy is an analysis technique used to measure the elemental composition of the surface of a material, elements that contaminate a surface, chemical or electronic state of each element in the surface, uniformity of elemental composition across the top surface, and uniformity of elemental composition as a function of depth in the material. XPS spectra are obtained by irradiating a material with a beam of X-rays while simultaneously measuring the kinetic energy and number of electrons that escape from the top 1 to 10 nm of the material being analyzed (http://en.wikipedia.org/wiki/X-ray_photoelectron_spectroscopy).

be etched with a rate of about 1 μm/hr. Finally, an HF wet and/or gas etch [Figure 6(d)] is used to remove the sacrificial oxide layer, leaving the diamond film suspended above the Si substrate.

Materials Integration Including UNCD Thin Films

Nucleation

"Seeding" is the term used to describe the processes employed to prepare a substrate prior to the growth of CVD diamond. In recent years there has been great progress in improving this process. The key figure of merit, the initial nucleation density, has improved in recent years from 10^{10} sites/cm^2 to 10^{12} sites/cm^2 [10]–[12]. The major advance has been the widespread adoption of nanocrystalline diamond powder (detonation nanodiamond or DND) and the use of ultrasonic techniques to distribute diamond nanoparticles of 2–10 nm in diameter uniformly on the substrate surface prior to growth. As a further improvement, Argonne researchers recently showed that the use of a thin 10-nm film of tungsten (W) greatly increased the nucleation density while also reducing the density of asperity defects on the surface (due to agglomeration of diamond seeds in one spot) [27]. Material properties such as the fracture strength [4], [5] and thermal conductivity [28] show clear improvements due to the enhancement of the interfacial bonding and reduction of voids and the formation of nondiamond bonding. If necessary, the very thin W layer can be later removed via wet etches using H_2O_2.

Stress

Compressive stress is ever present in diamond films grown onto silicon wafers due to the thermal expansion mismatch between diamond and silicon (1.1×10^{-6}/°C versus 3.2×10^{-6}/°C). However, UNCD films exhibit an unusually high intrinsic tensile stress that ranges from 200 to 400 MPa. This may be due to attractive forces between the diamond grains. This tensile stress nearly offsets the compressive component and frequently a residual stress for as-deposited films of approximately −100 MPa is observed. UNCD films also exhibit very low differential stress (down to 50 MPa/μm), due to both the microstructure. which does not vary with thickness, and the use of nanodiamond-based seeding techniques, which ensures uniform growth and density even in the first few layers of the film.

Electrodes and Electrical Contacts to UNCD

Standard Ti/Au/Ti metal stacks are incompatible with UNCD processing due to the relatively high temperature of deposition and the out-diffusion of Au, foiling the nucleation process. Alternatively we have successfully developed and implemented Cr/W stacks for electrodes in several different types of devices with success. The use of tungsten is further advantageous since it enhances the nucleation of the diamond itself. Furthermore, tungsten is widely used in CMOS interconnects, which again makes UNCD attractive for BEOL integration.

Metallic ohmic contacts were achieved on UNCD surfaces with sputter-deposited Al, Au, Cr, Cu, Pt, and Ti layers, all at a thickness of 200 nm [28], [29]. Current-voltage contact characteristics were used to calculate layer resistance from the slopes of these curves, including the resistance of the UNCD plus the resistance of the metal contacts themselves. When the contacts were all deposited on the same UNCD film, the difference in slope of the I-V curves were considered to be due to the change in the contact resistance alone. The most striking feature of the entire series of measurements was that every metal mentioned above forms a high-quality ohmic contact. While the total resistance changes with respect to metal and the use of an acid treatment, the R versus V curves are near perfectly linear in all measurements. Obviously, these results are important in terms of the implementation of electrostatically actuated UNCD-based RF MEMS/NEMS.
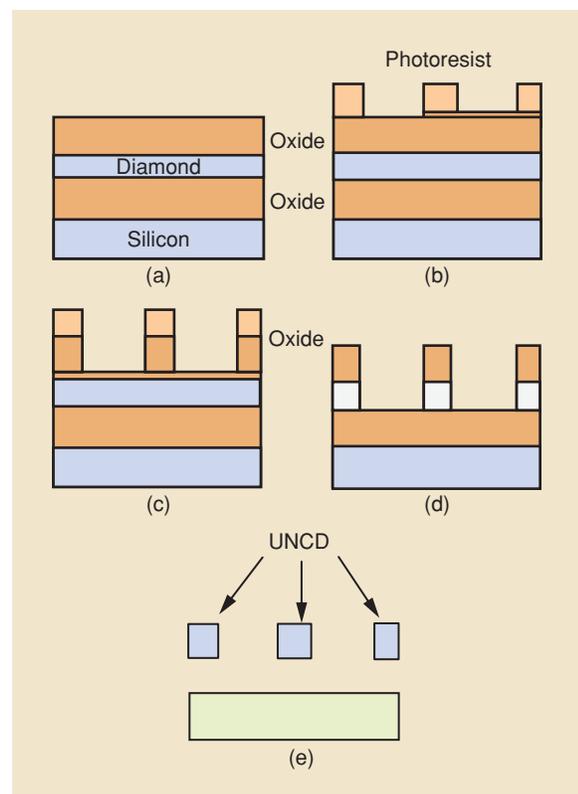
Figure 6. *Schematic showing lithographically-based process microfabrication of UNCD-MEMS: (a) deposition of UNCD on SiO$_2$ sacrificial layer plus masking layer; (b) and (c) photoresist and lithography; (d) reactive ion etching in oxygen plasma; (e) selective chemical etching of SiO$_2$ sacrificial layer. This process works very well because UNCD is not etched by any acid used in the fabrication of Si microchips or Si-based MEMS.*

Materials Integration for Piezoelectric UNCD-based MEMS/NEMS Actuators

Real estate is fast becoming a premium in most consumer-based mobile applications. In addition, the current evolution toward ever-decreasing power availability for such applications puts a severe strain on the current integration of electrostatic RF MEMS components with charge pumps needed to deliver 20–60 V. Such devices may become prohibitive in the future. Thus, alternative low-voltage actuation schemes are being explored as described in this section.

Low voltage RF MEMS/NEMS actuation can be achieved by sandwiching a piezoelectric material between two electrode layers on top of a structural beam layer. By applying a potential across the piezoelectric material, a strain is induced which in turn causes the structural material to deform in the same direction as the piezoelectric layer. In this respect, piezoelectric $Pb(Zr_xTi_{1-x})O_3$ (PZT) films, with excellent piezoelectric and electromechanical coupling coefficients and high remanent polarization, are being investigated for application to silicon-based MEMS devices [30], [31]. The piezoelectric coupling coefficients of PZT films are much higher ($e_{31,f} = -8$ to $-12C/m^2$ for epitaxial films) than those of other piezoelectric materials, such as ZnO ($e_{31,f} = -0.6$ to $-1C/m^2$) and AlN ($e_{31,f} = -1.05 \ C/m^2$) [31], [32]. Piezoelectric actuation of a 150-μm long cantilever beam, yielding deflections up to 5 μm, can be achieved with low voltages ($\leq$5 volts) with PZT film thickness of about 500 nm [33]. Since PZT has a relatively low Young's modulus (80 GPa) [34], it would not be an appropriate structural material for a RF MEMS/NEMS device such as a resonator. Thus, a high AV structural material integrated with a piezoelectric actuation scheme would be necessary for the realization of high-frequency devices with low-voltage operation.

Toward this goal, Auciello's group demonstrated recently [35] MEMS/NEMS piezoelectric actuators with UNCD as the structural material. A new materials integration strategy was required for an oxide piezoelectric layer such as PZT, which is generally grown by sputter deposition or metallorganic chemical vapor deposition (MOCVD) in an oxygen environment at relatively high temperatures ($\sim 600-750°$C). These growth processes would result in chemical etching of the carbon-based UNCD layer, via formation of volatile CO and CO_2 molecules. The work at ANL demonstrated that the PZT/UNCD integration can be achieved by using robust TiAl or TaAl (named TA) layers with dual functionality as oxygen diffusion barrier and adhesion layers interposed between the PZT and UNCD layers. The TA barriers were chosen based on thermodynamic arguments, which indicate that oxygen atoms react preferentially with Ti, Ta, and Al to form stable oxides due to the lowest energy of oxide formation for these elements with respect to all other elements in the periodic table [36]. The barrier functionality of TiAl layers was demonstrated in prior work on integration of
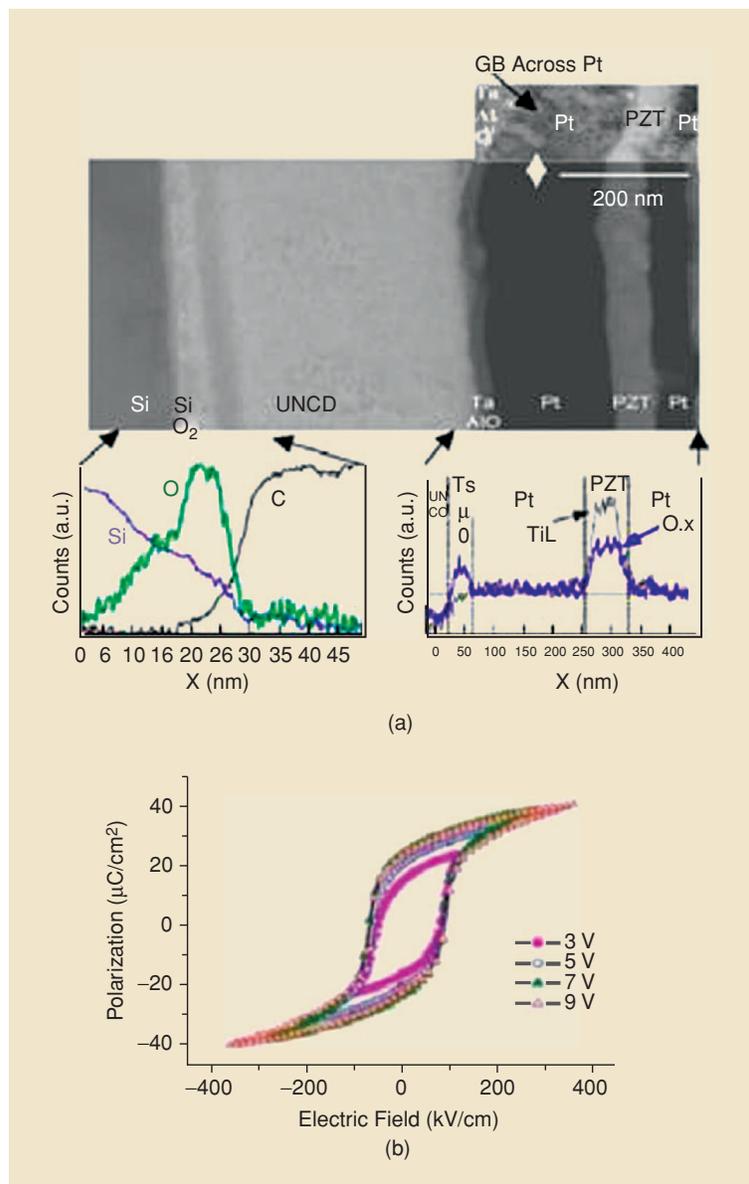
Figure 7. (a) Cross-section transmission electron micrograph (TEM) of a Pt/PZT/Pt/TaAl/UNCD heterostructure, showing the composition and microstructure of each layer and the interfaces. The bottom of the TEM image shows the compositional analysis of the different the different layers and the interfaces. (b) Polarization versus electric field for a Pt/PZT/Pt capacitor produced on a 1-μm thick UNCD layer.

$BaSr_xTi_{1-x}O_3$ films with Cu electrode layers to produce high-performance Cu/BST/Cu capacitors for high-frequency devices [37].

The materials integration developed by Argonne's researchers involved growth of a layered Pt/PZT/Pt heterostructure on UNCD MEMS cantilever actuators as a demonstration vehicle. A 1-μm UNCD layer was grown on a silicon substrate, using the deposition method described in the previous section. Subsequently, UNCD cantilevers were fabricated, using the photolithography plus RIE method described previously in this section. Finally, the diffusion barrier, electrodes, and PZT layers were deposited by magnetron sputter-deposition on the UNCD cantilevers. This deposition was done in an integrated cycle where all layers were deposited sequentially without breaking vacuum, thus providing good control of the deposition and layer integration process [35] [see Figure 7(a)]. PZT capacitors produced on UNCD displayed excellent ferroelectric properties as shown by the polarization versus voltage graph in Figure 7(b). Further details of the work performed to develop the PZT/UNCD integration can be found in [35].

The hybrid PZT/UNCD cantilevers were then tested in a dual-beam-focused ion beam (FIB) system with SEM capability. Figure 8 shows an SEM picture from a frozen frame of a movie recorded when actuating a hybrid PZT/UNCD cantilever with 5-V (ac) excitation in the range of 1 Hz to 1 MHz. This picture shows the hybrid cantilever at the second resonance (six resonances were demonstrated with oscillation amplitudes in the range of 1–4 μm). The cantilever was driven for 1 billion cycles, demonstrating the robustness of the PZT/UNCD hybrid structure.

This was the world's first demonstration of low-voltage piezoelectrically actuated diamond cantilevers. Work is currently in progress at ANL to optimize the materials integration strategy and fabrication processes of the actuator to design and produce high-performance piezoelectrically-actuated UNCD-based RF MEMS/NEMS resonators.

UNCD Integration in CMOS BEOL

Recently, Argonne, Freescale, and the University of Wisconsin-Madison researchers have demonstrated the integration of UNCD films with CMOS devices by growing UNCD films at 400°C on CMOS chips and testing them before and after UNCD growth. All devices were still performing to specifications with some degradation after UNCD deposition and processing. A threshold voltage degradation in the range of 0.08–0.44 V and transconductance degradation in the range of 1.5–17% were observed. Details of the integration strategy, electrical measurements, and possible mechanisms for the observed degradation will be published soon in a separate paper.

Demonstration of UNCD-based RF MEMS

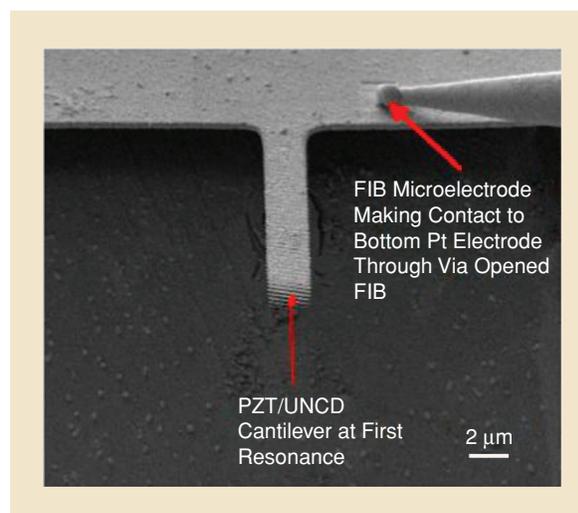### Electrostatically Actuated UNCD-based MEMS Resonators

Recently, several companies (SiTime, Discera) have announced the availability of silicon-based MEMS resonator-based products for timing applications. These devices exhibit very high performance in the low to mid MHz range but are unable to achieve the same reproducible performance in the high-MHz to low-GHz range. For such applications, silicon-based MEMS resonators usually require the use of higher-order modes [38]. Due to its extremely high acoustic velocity (twice that of silicon), UNCD promises to relax the design and manufacturing complexity of high-frequency resonators. As a first demonstration of UNCD-based resonators, simple fixed-fixed beam devices were fabricated. The fundamental mode resonant frequency for such devices can be written as [39]:

$$f_r = \frac{1}{2\pi}\sqrt{\frac{K_r}{m_r}} = \frac{1}{2\pi}\sqrt{\frac{K_m - K_e}{m_r}}$$
$$K_m = 16EW_r\left(\frac{h}{L_r}\right)^3$$
$$K_e = \frac{\varepsilon_0 W_r W_{el} V_d^2}{d^3},\qquad(1)$$

where K_r is the overall effective beam stiffness, K_m is the effective beam stiffness without any bias voltage present, K_e is the "spring softening" term related to the restorative force acting on the beam due to the application of the bias voltage, m_r is the effective mass of the beam, E is the Young's modulus, L_r is the beam length, W_r is the beam width, h is the beam thickness, W_{el} is the

FIB Microelectrode Making Contact to Bottom Pt Electrode Through Via Opened FIB

PZT/UNCD Cantilever at First Resonance

2 μm

Figure 8. *Scanning electron micrograph (SEM) of a hybrid PZT/UNCD MEMS cantilever vibrating at its resonance frequency, revealed by a frozen frame from a movie taken in a dual-beam focused ion beam (FIB) system.*

electrode width, V_d is the drive or bias voltage, and ε_0 is the permittivity of air. Note that in the special limiting case of applied bias $V_d = 0$, (1) is equivalent to the natural fundamental mode of the beam:

$$f_r = f_0 = 1.03 \sqrt{\frac{E}{\rho}} \frac{h}{L_r^2}, \qquad (2)$$

where ρ is the beam material density.

The UNCD MEMS resonator is fabricated via surface micromachining and the process is thoroughly described in [39]. Figure 9 shows a simplified schematic view of a completed resonator.

DC characterization was performed using a semiconductor parameter analyzer for beam breakdown, V_{bd}, (electrostatic breakdown or electromechanical pull-down) measurements. The pull-down voltage of resonator beams can be calculated as [40]:
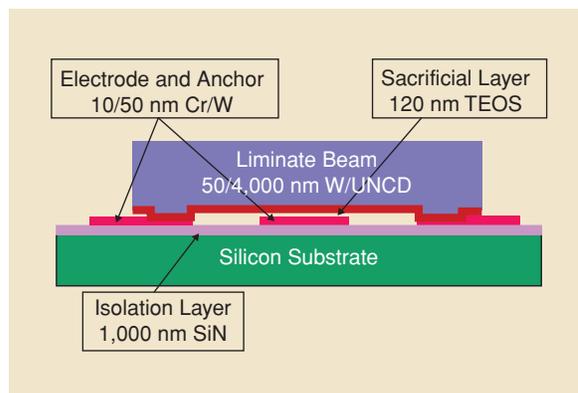
Figure 9. *Schematic cross section of a UNCD-MEMS fixed-fixed resonator device with typical process thickness of individual layers indicated.*
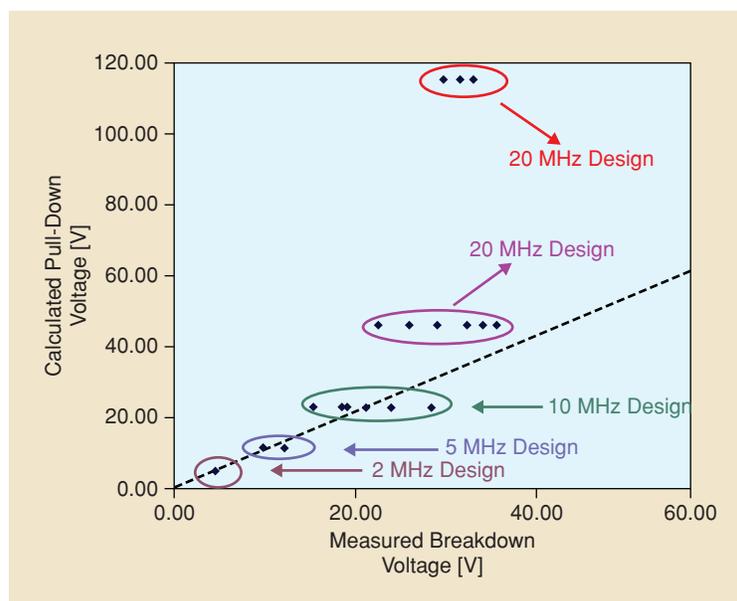
$$V_{pd} = \sqrt{\frac{8}{27} \frac{K_d d^3}{\varepsilon_0 W_r W_{el}}}$$

$$K_d = 32 E W_r \left(\frac{h}{L_r}\right)^3 \frac{1}{2 - \left[2 - \left(\frac{W_{el}}{L_r}\right)\right]\left(\frac{W_{el}}{L_r}\right)^2}, \qquad (3)$$

where K_d is the effective beam stiffness taking into account the distribution of the electrostatic force over the width of the biasing electrode. Figure 10 shows a comparison between calculated pull-down voltage and measured resonator breakdown voltages for various designs ranging from 2 to 50 MHz. With a gap of 120 nm the average electric field applied during pull-down tests for designs below 20 MHz are below the danger zone of approximately 200 V/μm for electrostatic breakdown in sub-micron vacuum gaps [41]. In contrast, both 20- and 50-MHz designs indicate breakdowns of around 30 V on average; suggesting electrostatic failure, not mechanical pull-down. Such breakdown behavior is strongly affected by the geometry (corners) and surfaces (roughness, work function) of the gap structures; hence small process variations and defects could lead to catastrophic failure of higher frequency devices. Although it has been shown that UNCD exhibits good electric field-induced electron emission, this only occurs at high vacuum levels of about 10^{-6} to 10^{-8} Torr [42]. Conversely, the dc characterization of UNCD-based resonators is done at atmospheric pressure where the mean free path of any electron emitted from the UNCD surface is negligible and therefore electrons would not be emitted or accelerated from that surface. Typical vacuum levels for RF MEMS resonators are around 1 to 50 mTorr, which would still be too low for field emission from the UNCD material. Based on these arguments, the authors believe that the observed breakdown is not due to field emission from the UNCD.

RF characterization was performed in a custom-built vacuum chamber with a base pressure of 20 mTorr. Again, no field emission issues were observed during testing. Both input and output RF signals are provided and measured by a vector network analyzer. The RF transmission spectrum (S21) is used to determine resonance frequency and quality factor Q of the device. Furthermore, a lumped element electrical model based on a force-voltage analogy is used to simulate the mechanical resonator as a series L-C-R resonant circuit. The model also includes the resonator static capacitance C_0, and parasitic elements such as bond-pad capacitance C_p and substrate resistance R_p [39]. Figure 11 shows a comparison of the measured and modeled RF

Figure 10. *Comparison between calculated pull-down voltage and measured breakdown voltages for various resonator designs ranging from 2 to 50 MHz.*

spectrum of a device with resonant frequency at 8.72 MHz. It is important to note here that the Q value of the resonator is relatively low. We believe this is due to a nonoptimal release etch process. At the present time, the devices are released via a wet etch and then coated with a thick resist protection layer for singulation. After singulation, the resist is removed and the individual die mounted and tested. This release/dicing process could potentially result in not completely "clean" structures. As indicated previously (see the "Bulk Properties" section), surface contamination can have deleterious consequences to the Q of such devices. However, measured Qs of ~10,000 have been observed for cantilever-type structures. Different options are being evaluated presently, from dry etching of the oxide sacrificial layer to the use of critical-point drying, in order to mitigate the issues with the current release etch process. Furthermore, new designs of free-free resonators are being fabricated and these should help in attaining higher Qs since anchor losses are minimized in such designs.

Figure 12 shows (a) the RF response of the resonator with varying bias voltages and RF power set at −10 dBm, and (b) the comparison between measured and modeled resonant frequencies for that same device. The total change in resonant frequency over the 15- to 25-V bias voltage range is 15.7%. Assuming a theoretical density of 3,500 kg/m^3, the derived UNCD Young's modulus from the model for both devices in Figures 11 and 12 is 710 GPa, which corresponds to an AV of 14,243 m/s. This value is close to the AV for the cantilever beam measured by Carpick's group (15,400 m/s). Even though the device designs and techniques used to the derived the AVs are quite different, the values show a percent difference of only 7.8%.

Equivalently, measurements were performed on the same device with varying RF power levels from −10 to 0 dBm with the bias voltage set at 20 V. The total resonant frequency variation over the range of RF power levels was 2.37%. This can be explained by the fact that the resonator "sees" an increased dc bias by the average voltage of the rectified RF signal as given by [43]:

$$V_{avg} = \frac{1}{T} \int_0^{T/2} V_p \sin(\varpi t)\,dt = \frac{V_p}{\pi}, \qquad (4)$$

where $T = 2\pi/\varpi$ is the period of the RF signal. The RF power in terms of peak voltage, V_p, given by:

$$P = \frac{V_p^2}{2Z}, \qquad (5)$$

where Z is the characteristic impedance of the electrode and for the frequencies of interest (10–50 MHz) is approximately 125 Ω. Using (4), and solving for V_{avg}, the following equation can therefore be used to determine the amount of average voltage derived from the RF power:

$$V_{avg} - \frac{\sqrt{2ZP}}{\pi}. \qquad (6)$$

From (6), the calculated average voltages for −10 and 0 dBm are 0.05 and 0.16 V, respectively. These voltages are small compared to the bias voltages and contribute to a small shift in frequency. However, RF power levels become critical for low bias devices, where the above average voltages are very close or above the pull-down/breakdown voltage. For example, assuming that the drive voltage V_d needs to be at least 50% of the pull-down voltage for adequate electromechanical coupling, and that the total voltage including the average voltage derived from RF power ($V_{tot} = V_{dr} + V_{avg}$) needs to be less than about 85% of the pull-down for reliability reasons, then the maximum allowable RF power for a 2-MHz device is 19 dBm or 77 mW. This clearly indicates a limitation in the applicability of such resonators, especially if they are intended to work as filters (diplexers/duplexers) in the transmit chain. This limitation will need to be addressed in more detail in the future.
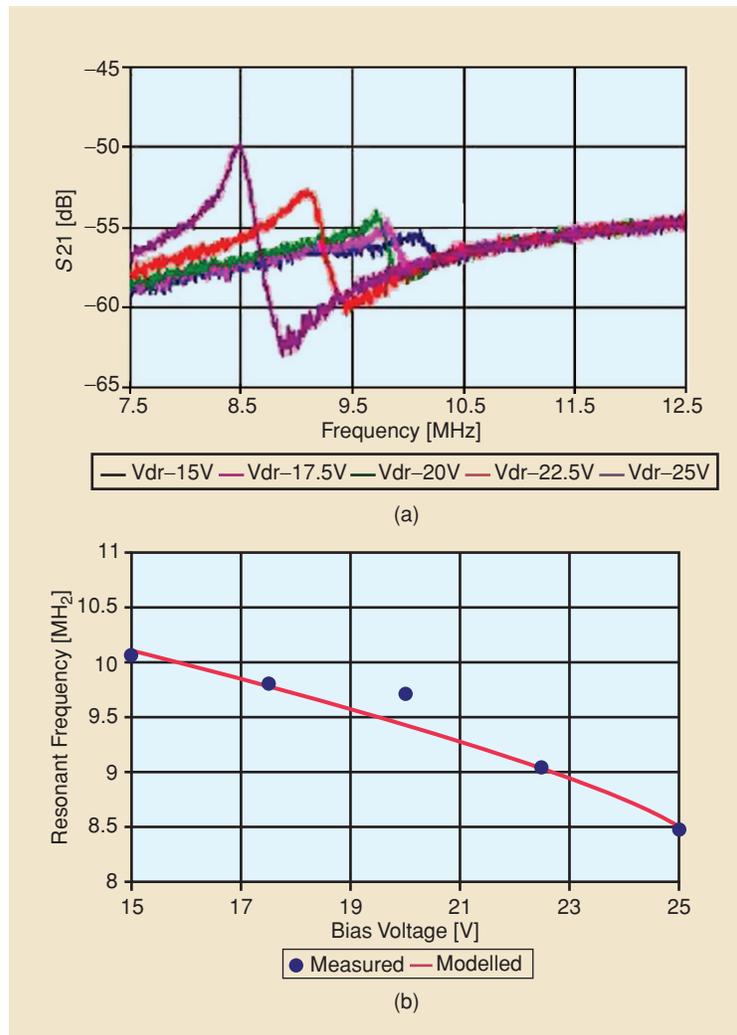
Several reproducibility measurements were performed on two different resonators by cycling the devices several times through varying bias voltage and RF power level conditions. The bias cycling measurements consisted of ramping the drive voltage from 15 to 25 V (in 2.5 V steps) at a power level of −10 dBm for a total of five cycles on a 10-MHz device. The RF power cycling consisted of increasing the power level from −10 to 10 dBm (in 5-dBm steps) at a bias voltage of 20 V for a total of three cycles on a 30-MHz device. Table 2 summarizes the maximum resonant frequency variation at each bias voltage and RF power setting (not to
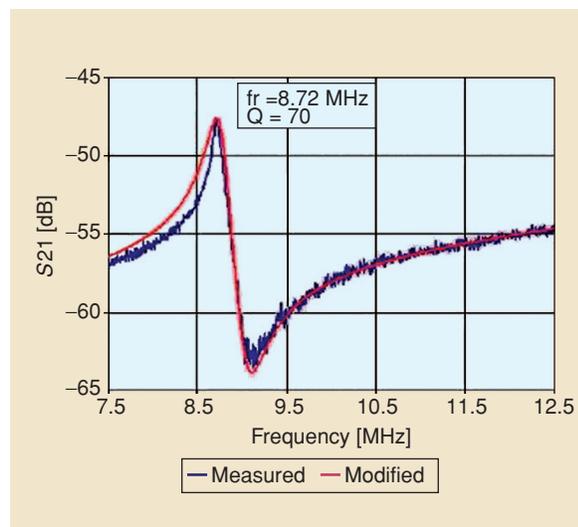
Figure 11. *Measured and modeled resonant frequency and Q of an UNCD device with a resonant frequency at 8.72 MHz. Measurements were performed with a drive voltage of 25 V and RF power level of −10 dBm. Model parameters are $E = 710$ GPa, $\rho = 3,500\,kg/m^3$, $h = 0.87\,\mu m$, and $d = 130$ nm.*

be confused with the change in resonant frequency as a function of applied bias). In both cases, the UNCD MEMS resonator shows acceptable reproducibility; however, prolonged measurements must be performed to determine the long-term stability of the devices.

This was a first demonstration of RF MEMS resonators built with UNCD films that were deposited at low temperatures (550°C). This low-temperature budget as well as the use of CMOS-compatible films and processing steps points toward future integration opportunities.

The Future for UNCD-based RF MEMS

A tremendous amount of extensive fundamental science has been done over the last decade to bring UNCD out of the lab and into the real world. This review has provided a glimpse of the capabilities of the UNCD film. The future for UNCD as a RF MEMS/NEMS functional material looks bright as its insertion will benefit specific applications where the film's exceptional properties will provide performance enhancements. UNCD's higher AV may relax the design and fabrication tolerances for resonators and thus provide a path to cost-effective volume manufacturing of timing references and oscillators. Its tribological and low-trap characteristics have the promise to further extend the reliability of RF MEMS switches. Furthermore, the low-temperature deposition capabilities currently being developed could enable fully integrated UNCD RF MEMS devices on the CMOS BEOL. However, much more work needs to be done in order to extract and reveal the full potential of UNCD. The authors are excited to continue the work in pushing UNCD technology to its fullest potential.

Acknowledgments

Figure 12. *Plots showing (a) RF response of UNCD resonator with varying bias voltages and RF power set at −10 dBm, and (b) comparison of measured and modeled resonant frequencies for the resonator in (a). Model parameters are $E = 710 \, GPa$, $\rho = 3,500 \, kg/m^3$, $h = 0.87 \, \mu m$, and $d = 127 \, nm$.*

TABLE 2. Maximum variation in resonant frequency at discrete BIAS voltages and RF power levels during cycling measurements.

Bias Voltage [V] (at −10 dBm)	Maximum Frequency Variation over Cycles 1–5 [%]	RF Power [dBm] (at 20 V)	Maximum Frequency Variation over Cycles 1–3 [%]
15.0	0.14	−10	0.14
17.5	0.47	−5	0.13
20.0	0.64	0	0.10
22.5	1.00	5	0.09
25.0	0.62	10	0.10
Average Variation [%]	0.57	Average Variation [%]	0.11

References

[1] K. Lim, S. Pinel, M. Davis, A. Sutono, C-H. Lee, D. Heo, A. Obatoynbo, J. Laskar, E.M. Tantzeris, and R. Tummala, "RF-system-on-package (SOP) for wireless communications," *Microwave Mag.*, vol. 3, no. 1, pp. 88–99, Mar. 2002.

[2] K.J. Gabriel, F. Behi, R. Mahadevan, and M. Mehregany, "In situ friction and wear measurements in integrated polysilicon mechanisms," *Sensors Actuators*, vol. A21–A23, no. 1-3, p. 184, 1990.

[3] A.P. Lee, A.P. Pisano, and M.G. Lim, "Impact, friction and wear testing of microsamples of polycrystalline silicon," in *Proc. MRS Symp.*, vol. 276, 1992, pp. 67-68.

[4] O. Auciello, J. Birrell, J.A. Carlisle, J.E. Gerbi, and X. Xiao, B. Peng, and H.D. Espinosa, "Materials, science, and fabrication processes for a new MEMS technology based on ultrananocrystalline diamond thin films,"*J. Phys.*, vol. 16, no. 16, p. R539, 2004.

[5] H.D. Espinosa, B.C. Prorok, B. Peng, K.H. Kim, N. Moldovan, O. Auciello, J.A. Carlisle, D.M. Gruen, and D.C. Mancini, "Mechanical properties of ultrananocrystalline diamond thin films relevant to MEMS/NEMS devices," *Exper. Mech.*, vol. 43, no. 3, p. 256, 2003.

[6] A.V. Sumant, D.S. Grierson, J.E. Gerbi, J. Birrell, U.D. Lanke, O. Auciello, J.A. Carlisle, and R.W. Carpick, "Toward the ultimate tribological interface: Surface chemistry and nanotribology of ultrananocrystalline diamond," *Adv. Mat.*, vol. 17, p. 1039, 2005.

[7] H. Takeuchi, A. Wung, X. Sun, R.T. Howe, and T-J. King, "Thermal budget limits of quarter-micrometer foundry CMOS for post-processing MEMS devices," *IEEE Trans. Electron Devices*, vol. 52, no. 9, Sept. 2005.

[8] B.V. Spitsyn, L.L. Bouilov, and B.V. Derjaguin, "Vapor growth of diamond on diamond and other surfaces," *J. Cryst. Growth*, vol. 52, p. 219, 1981.

[9] E. Kohn, P. Gluche, and M. Adamschik, "Diamond MEMS—A new emerging technology," *Diamond Relat. Mater.*, vol. 8, no. 2-5, pp. 934-940, 1999.

[10] A.V. Sumant, D.S. Grierson, A.R. Konicek, M. Abrecht, P.U.P.A. Gilbert, J.E. Butler, T. Feygelson, S. Rotter, and R.W. Carpick, "Surface composition, bonding, and morphology in the nucleation and growth of ultra-thin, high quality nanocrystalline diamond films," *Diamond Relat. Mater.*, vol. 16, no. 7, pp. 718-724, 2007.

[11] J. Philip, P. Hess, T. Feygelson, J.E. Butler, S. Chattopadhyay, K.H. Chen, and L.C. Chen, "Elastic, mechanical, and thermal properties of nanocrystalline diamond films," *J. Appl. Phys.*, vol. 93, no. 4, pp. 2164-2171, 2003.

[12] S.S. Rotter, "Growth of conformal thin diamond films by CVD for coating applications," in *Proc. Applied Diamond Conf./Frontier Carbon Technologies ADC/FCT '99*, Tokyo, 1999, p. 25.

[13] D.M. Gruen, S. Liu, A.R. Krauss, J. Luo, and X. Pan, "Fullerenes as precursors for diamond film growth without hydrogen or oxygen additions," *Appl. Phys. Lett.*, vol. 64, pp. 1502-1504, 1994.

[14] J. Birrell, J.A. Carlisle, O. Auciello, D.M. Gruen, and J.M. Gibson, "Morphology and electronic structure in nitrogen-doped ultrananocrystalline diamond," *Appl. Phys. Lett.*, vol. 81, p. 2235, 2002.

[15] X. Xiao, J. Birrell, J.E. Gerbi, O. Auciello, and J.A. Carlisle, "Low temperature growth of ultrananocrystalline diamond," *J. Appl. Phys.*, vol. 96 p. 2232, 2004.

[16] S. Jiao, A. Sumant, M.A. Kirk, D.M. Gruen, A.R. Krauss, and O. Auciello, "Microstructure of ultrananocrystalline diamond films grown by microwave Ar/CH4 plasma chemical vapor deposition with or without added H2," *J. Appl. Phys.*, vol. 90, pp. 118-122, 2001.

[17] S. Battacharyya, O. Auciello, J. Birrell, J.A. Carlisle, L.A. Curtiss, A.N. Goyete, D.M. Gruen, A.R. Krauss, J. Schlueter, A. Sumant, and P. Zapol, "Synthesis and characterization of highly-conductive nitrogen-doped ultrananocrystalline diamond films," *Appl. Phys. Lett.*, vol. 79, p. 1441, 2001.

[18] D. Zuiker, A.R. Krauss, D.M. Gruen, J.A. Carlisle, L.J. Terminello, S.A. Asher, and R.W. Bormett, "Characterization of diamond thin films by core-level photoabsorption and UV excitation Raman spectroscopy," in *Proc. Mat. Res. Soc.*, 1996, pp. 211-218.

[19] D.M. Gruen, A.R. Krauss, R. Csencsits, C.D. Zuiker, J.A. Carlisle, I. Jimenez, D.G.J. Sutherland L.J. Terminello, D.K. Shuh, W. Tong, and F.J. Himpsel, "Characterization of nanocrystalline diamond films by core-level photoabsorption," *Appl. Phys. Lett.*, vol. 68, pp. 1640-1642, 1996.

[20] A.V. Sumant, O. Auciello, A.R. Krauss, D.M. Gruen, D. Ersoy, J. Tucek, N. Moldovan, and D. Mancini, "Fabrication of MEMS components based on ultrananocrystalline diamond thin films and characterization of mechanical properties," in *Proc. MRS*, vol. 657, 2000.

[21] H.D. Espinosa, B.C. Prorock, and M. Fischer, "A methodology for determining mechanical properties of freestanding thin films and MEMS materials" *J. Mech. Phys. Solids*, vol. 51, no. 1, pp. 47–67, 2003.

[22] K. Johnson, J. Greenwood, and J. Colloid, "Adhesion map for the contact of elastic spheres," *Interface Sci.*, vol. 192, no. 2, p. 326, 1997.

[23] J. Birrell, J.E. Gerbi, J.A. Carlisle, O. Auciello, D.M. Gruen, and J.M. Gibson, "Bonding structure in nitrogen doped ultrananocrystalline diamond," *J. Appl. Phys.*, vol. 93, p. 5606, 2003.

[24] P. Zapol, M. Sternberg, L.A. Curtiss, T. Frauenhein, and D.M. Gruen, "Tight-binding molecular-dynamics simulation of impurities in ultrananocrystalline diamond grain boundaries," *Phys. Rev. B*, vol. 65, no. 4, p. 45403, 2002.

[25] R. Rameshan, "Fabrication of diamond microstructures for microelectromechanical systems (MEMS) by a surface micromachining process," *Thin Solid Films*, vol. 340, pp. 1-6, 1999.

[26] C.F. Chen, S.H. Chen, T.M. Hong, and M.H. Tsai, "Improvement of selectivity during diamond growth utilizing a new process" *J. Appl. Phys.*, vol. 77, no. 2, pp. 490-492, 1995.

[27] N.N. Naguib, J.W. Elam, J. Birrell, J. Wang, D.S. Grierson, B. Kabius, J.M. Hiller, A.V. Sumant, R.W. Carpick, O. Auciello, J.A. Carlisle, "Enhanced nucleation, smoothness and conformality of ultrananocrystalline diamond (UNCD) ultrathin films via tungsten interlayers" *Chem. Phys. Lett.*, vol. 430, p. 345, 2006.

[28] M.A. Angadi, T. Watanabe, A. Bodapati, X. Xiao, O. Auciello, J.A. Carlisle, J.A. Eastman, P. Keblinski, P.K. Schelling, and S.R. Phillpot, "Thermal transport and grain boundary conductance in ultrananocrystalline diamond thin films," *J. Appl. Phys.*, vol. 99, p. 114301, 2006.

[29] J.E. Gerbi, O. Auciello, J. Birrell, D.M. Gruen, J.A. Carlisle, and B.W. Alphenaar, "Electrical contacts to ultrananocrystalline diamond," *Appl. Phys. Lett.*, vol. 83, no. 10, p. 2001, 2003.

[30] D. Polla, "Electroceramic thin films, Part 2: Device application," *MRS Bull.*, vol. 21, no. 6, June 1996.

[31] P. Muralt, "Piezoelectric micromachined ultrasonic transducers for RF filtering and ultrasonic imaging," *Int. J. Computat. Eng. Sci.*, vol. 4, no. 2, p. 163, 2003.

[32] S. Trolier McKinstry and P. Muralt, "Thin film piezoelectrics for MEMS," *J. Electroceram.*, vol. 12, no. 1-2, p. 7-17, 2004.

[33] H-C. Lee, J-H. Park, J-Y. Park, H-J. Nam, and J.-Uk Bu, "Design, fabrication and RF performances of two different types of piezoelectrically actuated ohmic MEMS switches," *J. Micromech. Microeng.*, vol. 15, pp. 2098–2104, 2005.

[34] J. Akedo and M. Lebedev, "Piezoelectric properties and poling effect of Pb(Zr, Ti)O3 thick films prepared for microactuators by aerosol deposition," *Appl. Phys. Lett.*, vol. 77, no. 11, pp. 1710–1712, 2000.

[35] S. Sudarsan, J. Hiller, B. Kabius, and O. Auciello, "Piezoelectric/ Ultrananocrystalline Diamond Heterostructures for High-Performance Multifunctional Micro/Nanoelectromechanical Systems," *Appl. Phys. Lett.*, vol. 90, p. 134101, 2007.

[36] O. Knacke, O. Kubaschewski, and K. Hesselmann, *Thermochemical Properties of Inorganic Substances*, 2nd ed. Berlin: Springer-Verlag, 1991.

[37] W. Fan, S. Saha, J.A. Carlisle, O. Auciello, R.P.H. Chang, and R. Ramesh, "Layered cu-based electrode for high-dielectric constant oxide thin film-based devices," *Appl. Phys. Lett.*, vol. 82, no. 9, p. 1452, 2003.

[38] K. Wang, A.-C. Wong, and C.T.-C. Nguyen, "VHF free-free beam high-Q micromechanical resonators," in *Proc. IEEE MEMS Conf.*, Jan. 1999, pp. 453–458.

[39] S. Pacheco, P. Zurcher, S. Young, D. Weston, W. Dauksher, O. Auciello, J. Carlisle, N. Kane, and J. Birrell, "Characterization of low-temperature ultrananocrystalline diamond RF MEMS resonators," in *Proc. 35th European Microwave Conf.*, Oct. 2005, pp. 1523–1526.

[40] N.S. Barker, "Distributed MEMS transmission lines," Ph.D. disseration, Dept. Elect. Eng. Comput. Sci., Univ. of Michigan, 1999.

[41] T. Ono, Y. Dong, and M. Esashi, "Micro-discharge and electrical breakdown in a micro-gap," *J. Micromech. Microeng.*, vol. 10, no. 3, pp. 445–451, 2000.

[42] A.R. Krauss, M.Q. Ding, O. Auciello, D.M. Gruen, Y. Huang, V.V. Zhirnov, E.I. Givargizov, A. Breskin, R. Chechen, E. Shefer, V. Konov, S. Pimenov, A. Karabutov, A. Rakhimov, and N. Suetin, "Characterization of electron field emission properties in ultrananocrystalline diamond films," *J. Appl. Phys.*, vol. 89, pp. 2958–2967, 2001.

[43] S.P. Pacheco, "Design and fabrication of low actuation voltage K-bhnd MEMS switches for RF applications," Ph.D. thesis, Dept. Elect. Eng. Comput. Sci., Univ. of Michigan, 2004.